Appl. Phys. B 75, 203–214 (2002)
DOI: 10.1007/s00340-002-0968-7

Applied Physics B
Lasers and Optics

A.G. BEREZIN✉
O.V. ERSHOV
A.I. NADEZHDINSKII

Trace complex-molecule detection using near-IR diode lasers

Natural Sciences Center of General Physics Institute of Russian Academy of Sciences, 38 Vavilova St., 119991 Moscow, Russia

Received: 25 April 2002/Revised version: 29 May 2002
Published online: 21 August 2002 •

ABSTRACT The goal of the present paper was to develop an experimental technique to detect trace concentrations of complex molecules in the atmosphere using near-IR diode lasers. Ethanol and propane were chosen as model species. New optical, hardware, instrument-operation-mode and data-processing approaches for detection of trace complex molecules were developed. Different physical processes limiting the sensitivity of trace molecule detection were considered and solutions were developed to reduce the influence of these mechanisms on instrument operation. An absorption sensitivity of $\alpha_{\min} = 2.5 \times 10^{-5}$ for 4.5 ms measurement time was achieved, which is comparable with the sensitivity of "small" molecule detection. The first results utilizing this technique for in-field monitoring of trace complex molecules are presented.

PACS 33.20.Ea

1 Introduction

The first high-resolution molecular spectra using tunable diode lasers (TDLs) were recorded more than 30 years ago [1]. During the intervening decades, tunable diode laser spectroscopy (TDLS) was widely used in different areas of high-resolution molecular spectroscopy. A sample of the scope of activity can be found in [2], presenting papers from recent conferences TDLS-95, TDLS-98 and TDLS-2001.

Trace molecule detection using a TDL was considered as one of the most promising application of TDLS. The first demonstration of such an application was the open-atmosphere CO sensor [3]. The next important step towards highly sensitive trace molecular detection was achieved by J. Reid et al. [4] and increased significantly the sensitivity of resonant absorption detection using $2f$ detection. Various detection techniques used by different researchers (more than 400 publications during the last 20 years) demonstrated highly sensitive trace molecule detection with 0.1–1 ppb detection limits (see, for example, [5–9]). The majority of these results dealt with "small" molecules having spectra with resolved separated lines or multiplets. In contrast to "small" molecules, the line centers in the absorption spectra of complex molecules are located very close to each other (less than 10^{-3} cm^{-1}). This leads to overlapping of separate lines even at low pressures due to Doppler broadening and to formation of continuous band absorption spectra at atmospheric pressure.

Several approaches were developed to use TDLS for trace complex-molecule detection. To compare different techniques, $\alpha_{\min}$ – the minimum detectable absorption – is usually used. $\alpha_{\min}$ characterizes set-up parameters and the approach in use, and does not depend on a particular molecule or sample cell properties.

At low pressures, spectra of some complex molecules have fine structure, with characteristic widths of the spectral features close to the Doppler width. In [10], a spectral correlation function was proposed to detect trace complex molecules in absorption. This approach was then applied to detect trace freon-12 in the atmosphere [11] and BCl_3 in high-purity $GeCl_4$ [12]. (The English version of these results can be found in [13, 14].) As was shown in [13], the approach under consideration gives an improvement in sensitivity of $\sqrt{Z}$ with respect to single-line detection, where Z is the number of spectral features recorded. In these experiments, Z was about 10 000 and $\alpha_{\min} = 10^{-6} - 10^{-7}$ was demonstrated. The high density of lines in complex-molecule spectra in this case was transformed from a disadvantage (lines overlapping) to an advantage (huge number of recorded spectral peculiarities).

Ethanol has a similar spectra structure near 7.8 μ at low pressures. In [15], an ethanol detection technique was described using a quantum cascade laser (QCL) and multipass cell. It was the first demonstration of a very promising new laser type for trace-molecule detection. In the paper, absorption sensitivity was not mentioned, and using data presented we have estimated it to be $\alpha_{\min} = 2 \times 10^{-3}$.

With increasing pressure, the above-mentioned fine structure of the complex molecular spectra will be smoothed due to collisional broadening. Frequently, complex-molecule spectra have no fine structure even at low pressures (for example, see the ethanol band near 1.39 μ, below). At first sight it seems that such spectra cannot be detected by TDLS because they are much broader (100 cm^{-1}) than a typical TDL tuning range ($\Delta\nu \sim 1$ cm^{-1}). However, detailed investigation of complex molecular spectra has shown that many of them even at atmospheric pressure have rather narrow peculiarities of the order of a few cm^{-1}, being comparable with $\Delta\nu$. For instance, ethanol vapor has a narrow Q-branch near 1.392 μ, propane –

✉ Fax: +7-095/135-8281, E-mail: anber@nsc.gpi.ru

1.686 μ, dimethylhydrazine – 1.514 μ, etc. It is interesting to note that impurity spectra in liquids have similar widths.

In [16], we have demonstrated the possibility of detecting ethanol near 1.392 μ using this technique and algorithms developed for "small" molecules. The sensitivity achieved, $\alpha_{\min} = 3.3 \times 10^{-3}$, was mainly limited by environmental humidity variation and TDL temperature instability because of ethanol absorption overlapping with a strong water line.

Molecules with unresolved spectra mentioned above were introduced in [17] as broadband absorbers. The first broadband absorber detection using TDL was demonstrated by A. Mantz [18] more than 20 years ago, who used a TDL system with multiple wavelengths to detect impurities in plastics. Broadband spectral structure is of great importance for many applications for explosives, drugs and toxic-molecule detection. A straightforward approach is to use two lasers emitting in and out side of the absorption band of the molecule of interest. In [17], two TDLs operating near 1.65 and 1.31 μ were used to detect pyridine (C_5H_5N). Using data presented, we have estimated the absorption sensitivity as $\alpha_{\min} = 0.2 - 2 \times 10^{-3}$. Simultaneous detection of methanol and isopropanol was demonstrated in [19] using two lasers operating near 1.391 and 1.402 μ, utilizing the cavity ring-down (CRD) spectroscopy technique. CRD is a very promising technique for trace molecule detection. It is difficult to compare it with traditional methods because it compensates losses in absorption sensitivity by increases in optical length. In [19], the absorption coefficient sensitivity was estimated as $2.4 \times 10^{-9}\,\mathrm{cm}^{-1}$ and $\alpha_{\min} = 2 - 7 \times 10^{-3}$. It has to be mentioned that many of the applications at the moment need remote monitoring, where the CRD technique cannot be used.

As can be seen, at the moment the absorption sensitivity realized for broadband absorbers is 2–4 orders of magnitude worse than that typically needed for the detection of "small" molecules at atmospheric pressure and complex molecules at low pressure with a spectrum fine structure present, and not enough for trace complex-molecule detection.

Broadband absorbers represent the most difficult situation for trace molecule detection when no filtering procedures can be used. We consider the results below to be quite general. This paper describes an attempt to develop a technique of trace complex molecule (broadband absorber) detection. We pay special attention to developing a technique to be used in real applications where remote monitoring is required.

2 Experimental

2.1 *Molecular spectra*

It is very difficult to choose an optimal spectral range for any particular application because several aspects have to be taken into account, including the molecule itself, the laser and detector properties as well as the particular requirements of the application. We gave priority to the near-IR range for several reasons [16]. As remote monitoring is considered, eye safety standards [20] and glass transparency require the near-IR range. TDL and photodiodes for this spectral range are very reliable, commercially available and can operate at room temperature.

Although molecular fundamentals having the highest absorption coefficients are located in the mid-IR, this region is still inconvenient for applications because TDL and photodetectors need cryogenic cooling. In the near-IR range, one can find overtones and combination bands having 30–300 times smaller absorption than in the mid-IR. However, this loss of molecule absorption strength in some situations is overcompensated by an increase in photodiode detectivity. This is true for hydrogen bonds of many molecules. In the near-IR, one can find the first stretching overtones of several hydrogen bonds (OH – 1.4 μ, NH – 1.5 μ, CH – 1.7 μ, etc.). For other molecules, different spectral ranges have to be used. For example, a TDL operating near 7.8 μ is used to detect UF_6 (broadband absorber) [21].

Ethanol and propane, being representatives of molecules containing OH and CH bonds, respectively, were chosen to develop this technique of trace complex-molecule detection. Figure 1 shows transmission spectra of ethanol and propane in the near-IR range. Spectra were recorded using a Fourier transform spectrometer (FTS) Bruker 66-v with spectral resolution 0.25 and $0.5\,\mathrm{cm}^{-1}$ for propane and ethanol, respectively. The vapor over 98% liquid ethyl alcohol and a 5% gas mixture of propane in nitrogen were used. Propane contains only one CH bond and has its overtone band near $5800\,\mathrm{cm}^{-1}$ (the strongest feature near $5800\,\mathrm{cm}^{-1}$ in Fig. 1). In ethanol, both CH and OH bonds are present and absorption bands can be observed in both representative spectral ranges (weak band near $5800\,\mathrm{cm}^{-1}$ and a strong one near $7180\,\mathrm{cm}^{-1}$). Although the spectra have broad, unresolved features even at low pressures (broadband absorbers), rather narrow spectral peculiarities (marked by arrows in Fig. 1) enable TDLS usage for trace complex-molecule detection.

Figure 2 demonstrates a more detailed investigation of the ethanol spectrum. Transmission spectra of ethanol vapor were preliminarily recorded using the FTS "Bruker 66-v". A 25-cm long room-temperature cell was filled with ethanol vapor at different pressures from 0 to saturated pressure (38 Torr at $T = 18°$). The set of spectra recorded was used to obtain the ethanol spectrum presented in Fig. 2a. The cross section $K(\nu)$ determines the light transmission due to molecule absorption in the following way (no pressure dependence of $K(\nu)$ was

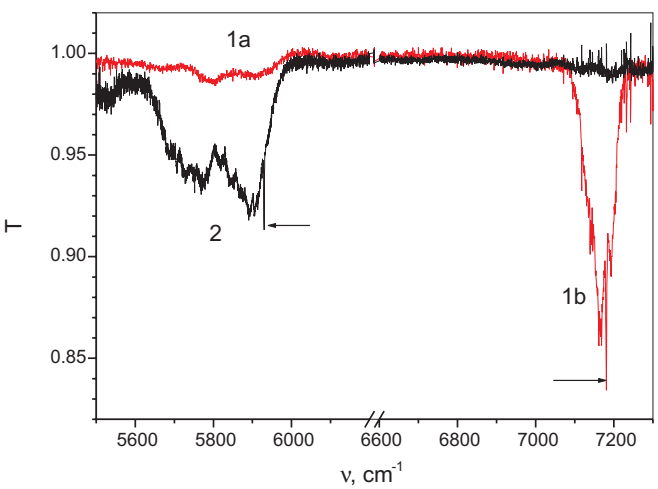

FIGURE 1 Transmission spectra – $T(\nu)$ of ethanol (1) and propane (2) in the near-IR range; ethanol: $L = 20$ cm, $P_0 = 30$ Torr, $C = 98\%$; propane: $L = 25$ cm, $P_0 = 760$ Torr, $C = 5\%$. *Arrows* indicate sharp spectral features

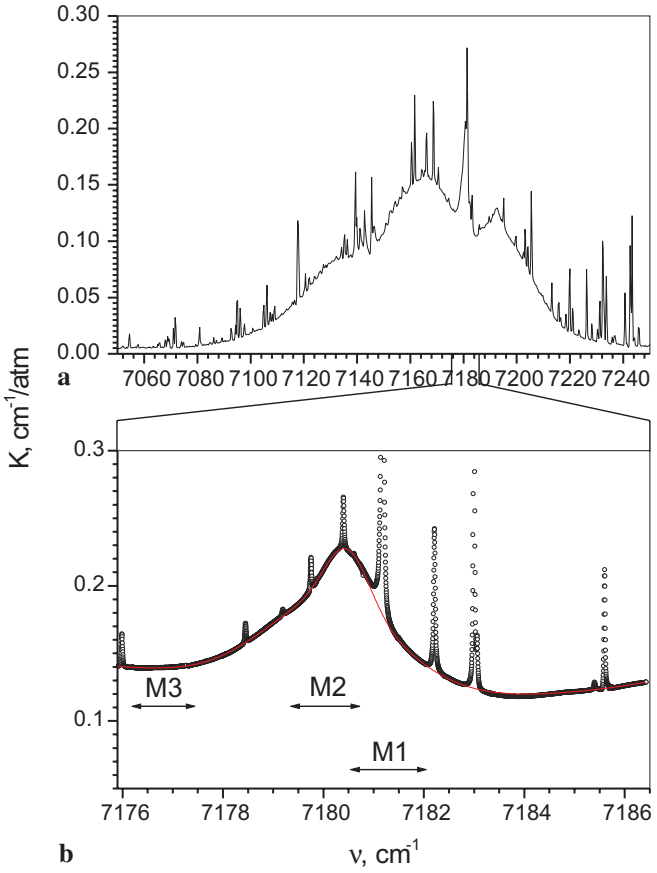

FIGURE 2 Room-temperature cross section spectrum $K(\nu)$ of ethanol vapor in the near-IR. **a** Spectrum recorded by FTS Bruker 66-v, resolution 0.25 cm^{-1}; **b** ethanol spectrum fragment obtained by TDL (*circles*) and spectrum model (*solid line*); M1, M2, and M3, spectral ranges selected for ethanol detection (see text)

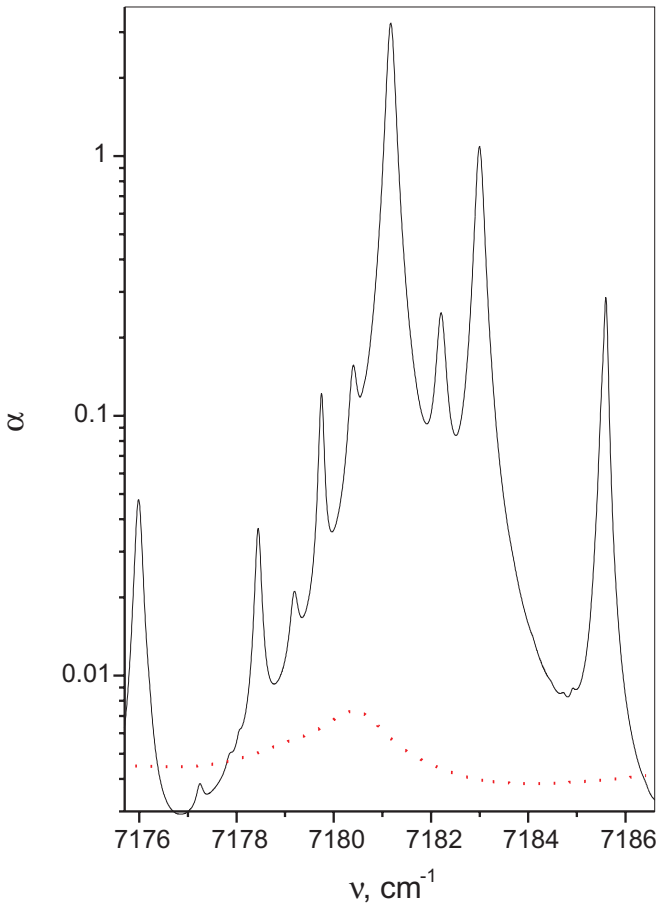

FIGURE 3 Absorption spectra – $\alpha(\nu)$ of water (*solid*) and ethanol (*dotted*) vapors in the atmosphere. $P_0 = 1$ atm, $L = 2$ m, $T = 18°$, 50% humidity, ethanol concentration $C_{C_2H_5OH} = 160$ ppm

experimentally observed):

$$T(\nu) = \frac{I}{I_0} = \exp[-\alpha(\nu)] = \exp[-K(\nu)P_0CL] \ , \qquad (1)$$

where $T(\nu)$ and $\alpha(\nu)$ are transmission and absorption spectra, respectively; I_0 and I are light intensities for the empty sample cell and the cell filled with a gas mixture, respectively; P_0 is the gas mixture pressure; C is the average concentration of the molecule under consideration; L is the- cell length; $P = P_0 \times C$ is the molecule partial pressure, $æ(\nu) = K(\nu)P_0C$ is the absorption coefficient. Below, CL is the integrated concentration and $c(x)$ is the local concentration at point x:

$$CL = \int_0^L c(x)\mathrm{d}x \quad . \qquad (2)$$

In the near-IR spectral range, a rather strong absorption band of ethanol was recorded within the spectral range between 7060 and 7220 cm^{-1}. This band represents the OH stretching overtone of the ethanol molecule and has a rather sharp Q-branch with HWHH (Half Width at Half Height) of approximately 1.3 cm^{-1} and a center near 7180 cm^{-1} (1.392 μm). A fragment of the ethanol spectrum near the Q-branch was obtained by TDL (Fig. 2b). Narrow absorption lines in Fig. 2 are due to trace H_2O in the non-dehydrated ethanol (98%) used in the experiment. The ethanol absorption in the spectral range under consideration has no fine structure even at low pressures. Four Gaussian functions were used to model the Q-branch shape (solid line in Fig. 2b).

Other compounds containing an OH bond also have absorption bands and lines within this spectral range. In this respect, when developing the methods of ethanol vapor detection one should pay special attention to measurement selectivity, especially, as concerns water vapor absorption that in real conditions significantly exceeds the absorption of ethanol vapor. The above is illustrated by Fig. 3, which shows the absorption spectra of water and ethanol in the vicinity of the ethanol Q-branch. The spectra were recalculated for the optical path length $L = 2$ m, atmospheric pressure $P_0 = 1$ atm, room temperature, 50% humidity, and ethanol concentration $C_{C_2H_5OH} = 160$ ppm (ppm – parts per million). As one can see, environmental water absorption is several orders of magnitude higher in comparison with that of the ethanol to be measured. Hence, ethanol is a good model on which to develop algorithms for trace absorption detection in the presence of the huge absorptions of other molecules.

To determine the optimal analytical range of the ethanol spectrum (Fig. 2), three ranges can be taken into account: 7180.5–7182 cm^{-1} (M1) having the maximum derivative, 7179.4–7180.8 cm^{-1} (M2) on the other side of the Q-branch

and M3 near 7176.5 cm^{-1} where there is no water absorption and ethanol has a flat spectrum. The first region, M1, is close to a very strong water absorption line and that is why it cannot be used in this application. In this respect, the second spectral range M2 with weaker water lines was selected for measurements.

3 Experimental set-up

Figure 4 shows a block diagram of the experimental set-up, consisting of an optical part, electronics and computer. Different variants of the optical part and its elements were developed and used in the present work. Radiation from the TDL module (1) was collimated by the objective (2). A beam splitter (1) deflected part (5–20%) of the laser beam into a reference channel (4), the rest of the TDL radiation was directed into an analytical channel (4). Gas cells as well as other optical elements (glass plates, diaphragms etc.) could be installed in the laser beam. Electronics was connected to (1), (4) and (5), and a computer was used to support instrument operation and data acquisition. The electronics contained a multifunctional input/output board (6) and interface analog module (7).

A set of various diode lasers, which emitted at the necessary wavelengths, was used in experiment. The majority of these lasers were manufactured by Nolatech Company (Moscow, Russia) and had Fabry–Pérot or distributed-feedback (DFB) resonators. We used also one DFB laser SU1392-DFB-TE from Sensors Unlimited Inc. (USA). The TDLs were assembled with a thermoelectric cooler/heater (TE) and temperature-sensitive resistor (thermistor). Some of the lasers were coupled to single-mode fibers. The usual

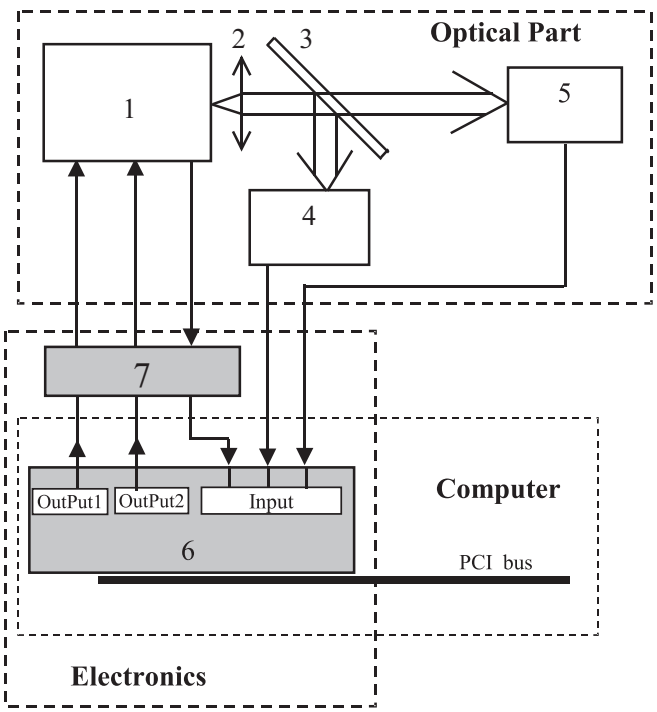

FIGURE 4 Block diagram of experimental set-up: 1, TDL module; 2, objective; 3, beam splitter; 4, reference channel; 5, analytical channel; 6, multifunction I/O board; and 7, interface module

TDL continuous-frequency tuning by pumping current was approximately 1 cm^{-1}. The TDL module was installed inside a plastic box, which was thermostatically controlled for better temperature stabilization.

The reference channel (4) contained a reference gas cell, photodetector and focusing optics. The rest of the optical scheme varied in different experiments. We used two main types of instrument optical layout. The first was built on an optical table. In this variant, the analytical channel laser beam was focused by a lens at a distance of approximately 250 cm from beam splitter (1) onto the photodetector. Gas cells with lengths 8.6, 12 and 200 cm could be installed in the laser beam in various experiments. Cells were filled with calibrated gas mixtures. An MKS Baratron gauge measured gas pressure. A second optical layout was used for open-path measurements. To reflect the laser beam into the analytical channel we used the following elements: a corner cube retro-reflector, scattering screen and a topography reflector. The distance between the instrument and the reflector varied from 1 to 45 m. Reflected TDL radiation was focused onto a photodetector with the help of a spherical or a parabolic mirror.

Ge photodiodes having a sensing area of 1.1 mm^2 with specially developed preamplifiers with third-order low-pass filters were used as photodetectors. The noise spectrum of each photodiode and preamplifier was measured and optimized for a particular application. Typical noise equivalent power (NEP) was 2×10^{-12} $W/Hz^{1/2}$ and the optimal bandwidth was found to be 30 kHz.

The National Instruments multifunction input/output board (NI-DAQ) PCI-MIO-16E-1 was installed into the computer PCI bus and connected through an interface analog module to the optical part of the instrument. Signals from a thermistor and two photodetectors in the reference and analytical channels were recorded by three NI-DAQ inputs. Two board outputs were used to control the TDL and the TE cooler/heater in the laser module. The board in use had 12-bit resolution. The input voltage range could be changed with the help of a programmable amplifier from (-50 mV $-$ $+50$ mV) to (-10 V $-$ $+10$ V). The board maximum operating frequency of 1 MHz was enough for the majority of experiments. The interface module amplified signals from the board outputs to necessary values for the TDL and TE currents, and provided a highly stable power supply for the preamplifiers.

The instrument operated under full computer control. Software was written using LabView 5.1. The NI-DAQ board produced repetitive pulses of TDL excitation current of any desired waveform that were generated by software and stored in the board's buffer memory. Temperature stabilization also was performed by software using the difference between the set value and the thermistor signal (thermistor temperature) and a proportional-integration regulation algorithm. The feedback signal generated by the computer through the analog interface was directed to the laser module TE cooler/heater. A temperature stability of approximately 2×10^{-3} K was obtained could be considered as typical for TDLS.

4 Operation mode

The intensity of TDL radiation and its frequency depend on both the TDL temperature and the laser excita-

tion current. Various TDL operation modes are used for trace molecule detection. Below, we shall describe the technique we developed and used in our laboratory. It is well known that in TDLS physical processes, the limiting sensitivity of trace molecule detection has a flicker-type nature (see, for example, [7]). For flicker-type noise, the optimum strategy is to perform a single measurement as soon as possible and then to average the subsequent signals measured.

According to this strategy, short, repetitive current pulses excited the TDL. The waveform of each photodetector signal period was separately recorded and processed and only after processing were they averaged over the train of pulses. As was mentioned above, the computer can generate any TDL excitation-current waveform. Three examples of photodetector signals for different excitation-current waveforms used are shown in Fig. 5. The TDL temperature was chosen so that the radiation frequency was near the maximum of an ethanol Q-branch. The sharp resonant features observed in Fig. 5 are due to narrow spectral lines of water, as a cell filled with low-vapor-pressure water was installed into the laser beam. Area "0" corresponds to excitation current below the threshold. It is very convenient to have this option to subtract background radiation. Moreover, it is critically important in some cases, for example, when the instrument receives only a very small part of the laser light scattered from the topography reflector, superimposed by a huge background radiation [22]. Areas "S" and "D" were used for laser frequency tuning stabilization (see below) and trace absorption detection.

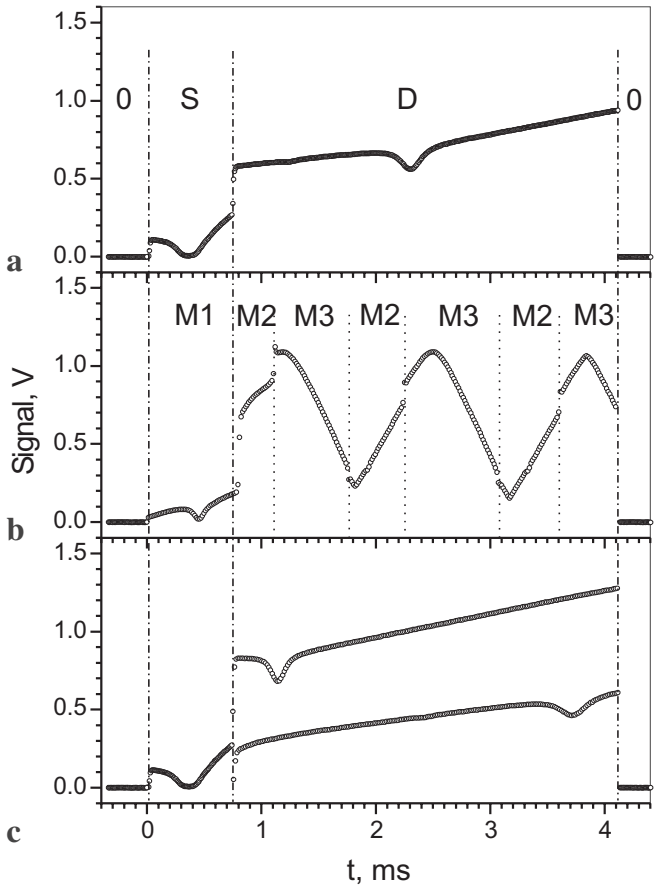

FIGURE 5 Photodetector signal waveform examples. Areas 0, S and D were used for background subtraction, stabilization of laser frequency tuning cycles and trace-molecule detection, respectively; M1, M2, and M3, three spectral ranges selected for ethanol detection (see text)

The signal shown in Fig. 5a was used in our spectroscopy experiments. An excitation-current waveform for this case had the traditional trapezoidal form. Results presented in Fig. 2 were obtained using this mode. The same waveform was used in [16] to detect ethanol. However, such a waveform is not optimal for trace-molecule detection, especially when complex molecules are considered, because of the influence of flicker noise. The signal shown in Fig. 5b demonstrates another possible use of TDL properties. The excitation-current waveform of the pulse consisted of a constant current with a few periods of sawtooth function superimposed on it. For this waveform, the TDL emitted radiation in all three spectral ranges (M1, M2 and M3) mentioned in Sect. 2.1. When excitation current was increased, the TDL in use changed its operation from one laser mode (M2) to another (M3), shifted by $4\,\mathrm{cm}^{-1}$. Because of TDL bi-stability, mode hops occurred at different excitation currents when the current was increased or decreased. Hence, two different waveform slopes are presented in Fig. 5b. The TDL radiated at different frequencies shifted by $4\,\mathrm{cm}^{-1}$ with respect to each other. In our experiments with different lasers, we observed similar mode-hop behavior with higher frequency differences (up to $50\,\mathrm{cm}^{-1}$). Such a TDL operation mode is interesting when taking into account the spectral structure of broadband absorbers, because it provides an increase in the spectral range. In contrast, we observed the presence of significant instabilities at the location of mode hops, typical for such laser operation, which is not very good. Finally, Fig. 5c shows a signal that we consider to be the most attractive for trace-molecule detection. In this case, the TDL emitted in one laser mode. In area "D", excitation current quickly switched from one trapezoidal waveform to another. In the particular mode shown in Fig. 5c, the period of switching was chosen to be equal to two data-sampling periods. If this mode was in use, one could see the signal with rectangular modulation on an oscilloscope, while the recorded signal looked like two different data sets of odd and even signal points. Any number of data sets could be obtained by varying the ratio (integer) of switching period and data-sampling time.

Let us consider the optimum time parameters for the TDL waveform presented in Fig. 5c. Thermal processes in the laser active area determine the TDL radiation properties [23]. There are two characteristic times t_1 and t_2 that can be experimentally obtained for each laser in use. For $t < t_1 \approx 10\,\mu\mathrm{s}$, excess noise and instability of radiation will occur due to inhomogeneous temperature distribution in the laser active area (random distribution of excitation current density together with inhomogeneous current carrier mobility [24]). For $t > t_2 \approx 1\,\mathrm{ms}$, long-term changes of laser contact properties influence the temperature distribution in the laser active area, and these provide additional radiation instability. Hence, the optimal timescale of the TDL waveform is between $10\,\mu\mathrm{s}$ and 1 ms. With this in mind, we used a data sampling time of 5–15 μs and a pulse duration of 100–500 μs for trace absorption detection. For precise molecular spectral recording or for presentation purposes, higher pulse du-

rations have been used as is shown in Fig. 5. For ethanol detection, long pulses were also used to generate more data points for better operation of the orthogonalization procedure (see Sect. 2.4).

Figure 6 illustrates the operation of the system under consideration. The signal waveform in the "D" area of Fig. 5c is shown in Fig. 6a. Figure 6b presents the absorption α calculated using the two signals recorded: the first one when the sample cell ($L = 200$ cm) was empty-I_0 (not shown), and second one when it was filled with ethanol vapor ($P_0 = 21$ Torr, $C = 98\%$)-I (shown in Fig. 6a), with the help of (1). The slow varying part of α is determined by ethanol (Fig. 2), while the narrow lines are due to trace water absorption. The TDL frequency tuning $\nu(t)$ presented in Fig. 6c was calibrated using the known water line frequency $\nu_0 = 7180,3998\,\mathrm{cm}^{-1}$ [24] (dot horizontal line), Fabry–Pérot etalon spectrum and the functional dependence described in [23]. It looked like the laser radiated "simultaneously" at two frequencies and these frequencies were tuned during the laser pulse corresponding to the two data sets in Fig. 6a and b. It is obvious from Fig. 6c that the same water line was observed in the two data sets of the present waveform denoted by the vertical dash-dot lines, and the maxima of the slowly varying part of each data set correspond to the ethanol Q-branch maximum. Different water line widths in the two data sets are due to different slopes of $\nu(t)$ (Fig. 6c). Laser frequency tuning was determined for each of the instrument parameter sets in use and stored in the computer memory.

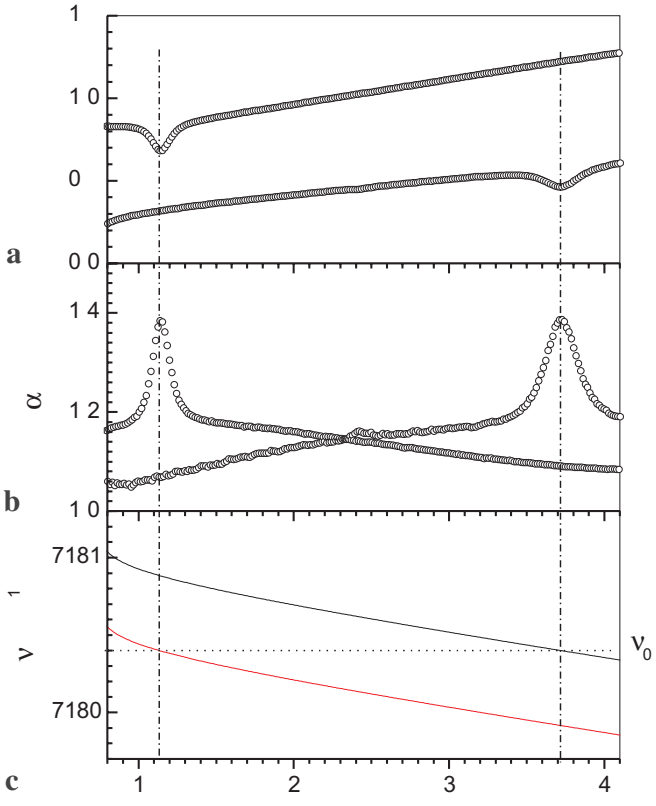

FIGURE 6 Recorded signal waveform (**a**), detected ethanol absorption, α (**b**), and laser frequency tuning, $\nu(t)$, (**c**) (see text); ethanol: $L = 200$ cm, $P_0 = 21$ Torr, $C = 98\%$

Our experiments with ethanol [16] showed that the TDL temperature stability is of great importance for trace complex-molecule detection. Variations of TDL temperature should lead to a vertical parallel shift of $\nu(t)$ (Fig. 6c) and the changing of the spectral line position within the pulse. Figure 7 (left) shows laser frequency instability $\nu - \nu_0$ (ν_0-frequency of spectral line) measured using the spectral line position. A laser frequency variation with a standard deviation $\mathrm{std}(\nu - \nu_0) = 1.6 \times 10^{-3}\,\mathrm{cm}^{-1}$ was observed when a thermistor was used as the temperature sensor. Taking this value into account the environmental water absorption data (see Fig. 3) and the experimental conditions used in [16], the absorption sensitivity can be calculated as $\alpha_{\min} = 2.4 \times 10^{-3}$, being close to the sensitivity results mentioned in the paper. The traditional stabilization scheme presented above has an important disadvantage. It stabilizes the thermistor temperature rather than the diode laser temperature. The trend in Fig. 7 is typical for such a TDL temperature stabilization scheme because there is no ideal thermal contact between the thermistor and the TDL.

Stabilization of TDL frequency tuning cycles $\nu(t)$ using the spectral line position was proposed in [26] and provided significant improvement in TDLS precision. In this approach, $\nu(t)$ (see Fig. 6c) is stabilized at one point of the laser pulse. TDL frequency instability in this point is also shown in Fig. 7 (right). The difference between the measured spectral line position inside the pulse and the set value was used; the remaining part was the same as described above for temperature stabilization. For this stabilization scheme, a ten-times improvement in stability was observed with $\mathrm{std}(\nu - \nu_0) = 1.5 \times 10^{-4}\,\mathrm{cm}^{-1}$. In our experiment we used a signal from the reference channel with a 25-cm cell filled with low water vapor pressure. To increase water absorption, the spectral range M1 with the strongest water line was used (Fig. 5). The frequency stability obtained was of the same order as that in [26], taking into account the difference in Doppler line width in the mid- and near-IR ranges. Long-term instability of frequency tuning was observed. The slope of frequency tuning $\nu(t)$ and the difference between the two frequency sets changed with a characteristic time of around 30 min. This effect was compensated by a tuning frequency calculation in real time using the position of all the spectral lines observed in the recorded signal (Fig. 6a).

5 Data processing

Two signals similar to the one shown in Fig. 5c were used in data processing. The first was the signal under consideration, i.e. the analytical signal. The second signal had to be recorded without the molecule under investigation in the laser beam. During the preliminary step of data processing, the background signal levels obtained for area "0" were subtracted from both signals. Area "D" of the resulting signals formed two arrays $I(i)$ and $I_0(i)$ ($i = 1....N$) (Fig. 6a).

Further data processing includes: 1 – calculation of the absorption array $\alpha(i)$ using (1) (Fig. 6b); 2 – separation of even and odd points in $\alpha(i)$ resulting in two arrays $P1$ and $P2$, corresponding to the two data sets mentioned above; 3 – interpolation of these arrays for all data points ($i = 1...N$); 4 – calculation of the analytical signal $A(i)$ ($A = P1 - P2$)

(A is the difference between the two data sets in Fig. 6b); 5 – calculation of the ethanol function $E(i)$ using the ethanol spectrum model (Fig. 2) and $\nu(t)$ determined; 6 – determination of the water function $W(i)$ using the recorded water vapor absorption spectrum; 7 – calculation of correlation factors between array A and arrays E and W using orthogonalization procedure; and 8 – calculation of ethanol and water concentrations.

Calibration steps 5 and 6 may be done either once in advance and stored in the computer memory, or each time. The experimental determination of the ethanol function E is very complicated, contains many steps and is not reliable because of the presence of narrow water lines (Fig. 6b). For this reason, the calibration procedure is based on the ethanol spectrum model (see Fig. 2b solid line). We did not use the HITRAN [25] database to calculate the water function W because the difference between the experimental water spectrum in this spectral range and the spectrum calculated using HITRAN data was too large. In contrast, the experimental W determination was rather quick and simple. Two signals were recorded to obtain W with a reflector installed at two different distances from the instrument.

The data processing technique described above made the final result insensitive to several disturbance factors in trace absorption detection: preliminary step – insensitive to background radiation variations being slow with respect to the signal period (100 μs–5 ms); step 1 – insensitive to the TDL baseline; step 4 – insensitive to the TDL intensity variations being slow with respect to the sampling time (5–15 μs); step 7 – insensitive to environmental water concentration variations. The procedure demonstrated for ethanol detection is valid for all broadband absorbers. We also used it with some modifications (data filtering) for small molecule detection.

The software developed allowed independent treatment of each signal pulse (rapid monitoring mode). Thus, the minimum duration of one measurement of molecule concentration could be as quick as the pulse repetition period. Averaging over a train of pulses led to noise reduction.

6 Results

The analytical array A can be presented as:

$$A\,(i) \;=\; P_0 CL \times E(i) + a(i); \quad i = 1, ..., N \quad . \tag{3}$$

Here, $a(i)$ is the signal noise or disturbance component.

Noise limits detection sensitivity. Minimum detectable concentration, $C_{\min}$, and absorption, $\alpha_{\min}$, can be determined (if white noise is considered) for data processing in use:

$$C_{\min} \;=\; \frac{1}{P_0 L}\sqrt{\frac{1}{N}\sum_{i=1}^{N} a(i)^2 \Big/ \sum_{i=1}^{N} E(i)^2}$$
$$= \frac{\mathrm{std}(a)}{P_0 L\sqrt{N}\times \mathrm{std}(E)}; \quad \acute{a}_{\min} \;=\; \frac{\mathrm{std}(a)}{\sqrt{N}} \quad . \tag{4}$$

Here, std(E) is the standard deviation of the ethanol function array $E(i)$.

$C_{\min}$ characterizes the sensitivity of the particular system to detect a given molecule. To characterize experimental results presented in this section, we shall use the minimum detectable molecule partial pressure in the gas mixtures under investigation – $P_{\min} = P_0 C_{\min}$. This value was experimentally measured when sample cells were filled. Integrated concentration – $C_{\min} L$ (see (2)) is frequently used to characterize molecule detection sensitivity. This value is insensitive to the sample cell or open-path length (traditionally its unit is ppm× m). $\alpha_{\min}$ was mentioned in the introduction and $æ_{\min} = \alpha_{\min}/L$ determines the minimum detectable absorption coefficient.

6.1 *Laboratory test*

We performed a calibration test on both the developed instrument and the detection procedure for trace broadband absorbers. Below, we shall demonstrate results for ethanol, because experiments with ethanol are more difficult in comparison with propane and many other complex molecules. Calibrated gas mixtures with known ethanol partial pressures P were used for calibration. Before each measurement, the reference signal was recorded with the sample cell ($L = 8.6$ cm) filled with environmental air. Then the cell was evacuated and filled with a different ethanol pressure – P (calibrated pressure below) from 0.5 to 31 Torr. Ethanol vapor over 98% liquid ethyl alcohol was used as the ethanol source. The spectrum of such a sample at low pressure contains narrow water lines and cannot be used for calibration. Atmospheric air was added to the cell to bring the total pressure to $P_0 = 1$ atm. This procedure had to be slow enough to prevent ethanol condensation on the cell walls.

We averaged over 120 waveform periods with a measurement time of 0.5 s. The ethanol partial pressure was determined using a data processing procedure (see Sect. 2.4) and is presented in Fig. 8 as a calibration function for the gas mixtures used. A linear fit (solid) with 95% confidence lines (dotted) demonstrates good technique linearity. The correlation coefficient between calibrated and measured ethanol partial pressures was 0.990 ± 0.015. Difficulties in the preparation of calibrated gas mixtures (ethanol condensation) were responsible for the standard deviation of the difference between experimental points and linear fit – 0.26 Torr. The standard

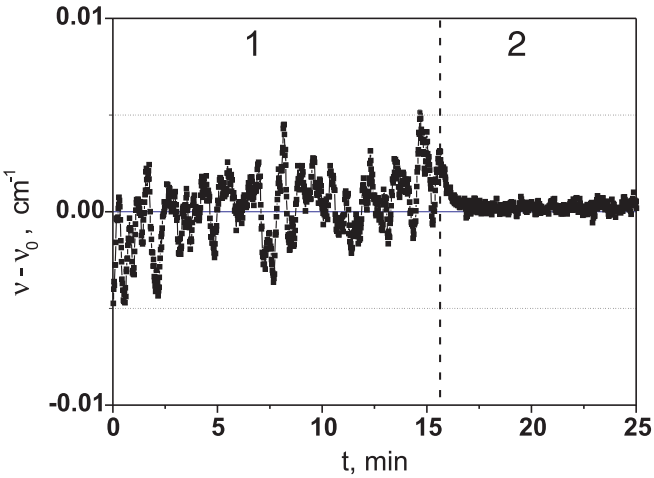

FIGURE 7 TDL frequency instability, $\nu - \nu_0$, when thermistor signal (1) or spectral line position (2) were used for feedback to TE

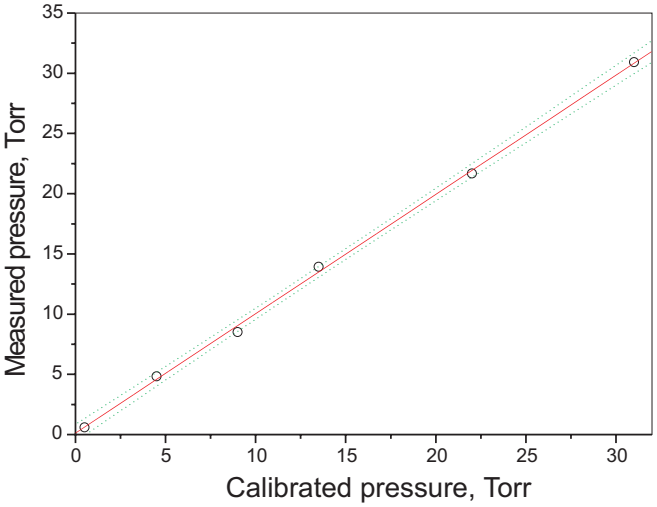

FIGURE 8 Measured ethanol partial pressure in calibrated gas mixtures vs. calibration mixture, *circles* – experiment; *solid* – linear fit, *dotted* – 95% confidence; $L = 8.6$ cm, $P_0 = 1$ atm

deviation of the measured partial pressure for a given calibrated mixture had the smaller std of 0.16 Torr.

An example of ethanol monitoring presented in Fig. 9 was obtained using a bubbling technique. The sample cell ($L = 8.6$ cm) was installed in the TDL beam and was connected to a volume with a calibrated water–ethanol solution. Slow (0.1 l/min) atmosphere gas flow through the solution provided a gas mixture with a reproducible water and ethanol concentration. We used two volumes, one with distillated water and other one with an ethanol–water solution (10 %vol.) and we were able to connect each of them to the sample cell. All other experimental details were the same as those given above. The experiment presented in the figure started with the water volume connected to the cell. The reference signal was recorded at that time. When volumes were replaced, one can observe increasing or decreasing of ethanol integrated concentration – *CL*. Half a minute was needed to replace the cell volume content with the slow gas flow technique. The measured ethanol integrated-concentration value recalculated

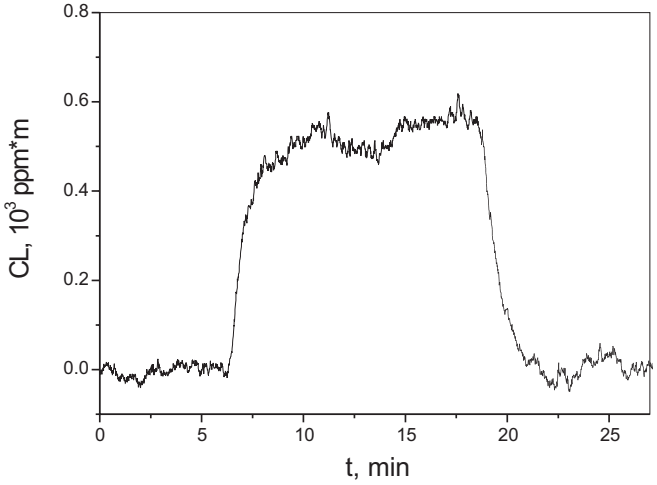

FIGURE 9 Ethanol integrated concentration *CL* monitoring using the bubbling technique; $L = 8.6$ cm, $P_0 = 1$ atm

to ethanol concentration in solution – 9.6 ± 0.6 %vol. – was in good agreement with the calibrated one – 10 %vol. (preliminary equilibrium ethanol partial pressure was determined using the same bubbling technique and FTS; interesting aspects of ethanol partial pressure thermodynamics above solutions were considered in [27].) The minimum detectable integrated concentration was found to be $CL = 17$ ppm × m. This value corresponds to a minimum detectable ethanol partial pressure $P_{\min} = 0.15$ Torr, similar to the calibration test. Sensitivity limitations (see Fig. 9) were caused by the rather slow processes. At the same time, the slow variation of the analytical signal A baseline was observed in real time on the computer screen. (Hence, sensitivity limitations in the present experiments were related to the slow analytical signal baseline variations).

An example of the rapid monitoring mode is shown in Fig. 10. Each point is the result of an ethanol measurement during one signal period (4.5 ms). Here, the laser beam crossed a sample cell filled in the same way as during the calibration test. The cell was filled by environmental air (left) and gas mixture ($P = 9.6$ Torr of ethanol in air) (right). Figure 10a and b presents transmission T and ethanol integrated concentration – *CL*, respectively. In Fig. 10a, one can see transmission variation when the beam crossed the cell: 100% transmission when there was no cell in the beam, its reduction to 0% due to the cell walls, and some reduction because

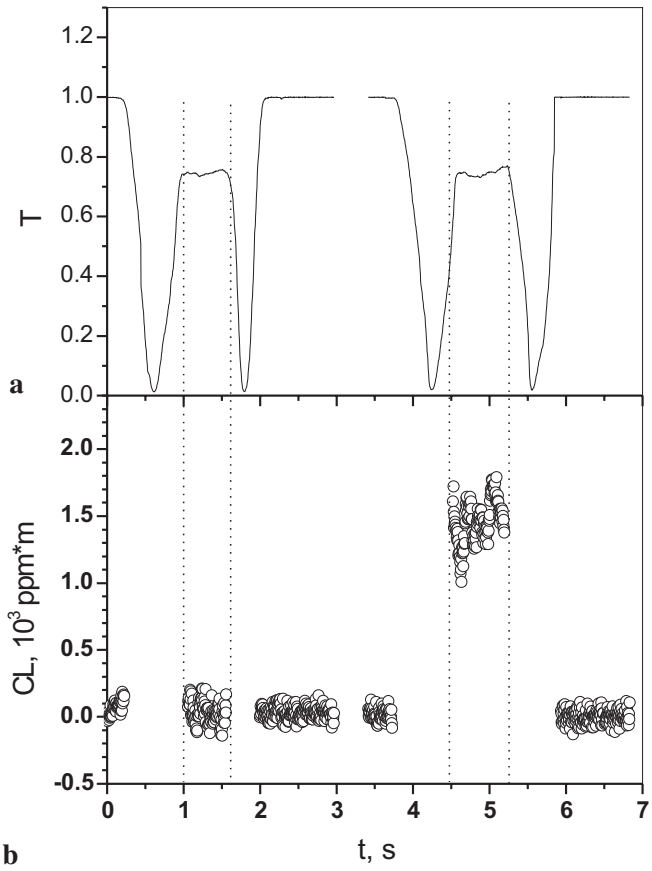

FIGURE 10 Transmission, T (**a**) and ethanol integrated concentration, *CL* (**b**) measurements when laser beam was crossed by sample cell filled with environmental air (*left*) and gas mixture (9.6 Torr of ethanol in air) (*right*); $L = 12$ cm, $P_0 = 1$ atm

of light reflection by the cell windows when the beam passed through the cell. When the first reduction in transmission was detected, the software stored the signal prehistory in the computer memory, calculated the reference signal, then recorded the signal for some period of time (3 s for data presented), and processed the data recorded. Additional noise can be observed when a moving cell crossed the laser beam. Results presented here were obtained with the cell having the lowest noise. For other cells in use, noise was several orders of magnitude higher. Minimum detectable integrated absorption $C_{\min}L = 45$ ppm $\times$ m was determined. It was limited by the 12-bit ADC resolution, because change in the ADC programmable amplifier limits was followed by proportional noise increase. Obtained $C_{\min}L$ value has to be compared with 18 and 17 ppm $\times$ m (Figs. 8 and 9, respectively) obtained by averaging of 120 signal periods. Due to signal averaging, influence of ADC resolution has to be reduced 11-times. The final improvement in sensitivity after averaging was smaller than that predicted because of flicker-type noise presence (see Fig. 9).

7 Absorption detection sensitivity

In the present section we shall consider different processes that limited absorption sensitivity. Significant recorded signal variations due to optical misalignment, atmospheric turbulence, etc. together with the broad, unstructured spectrum of complex molecules prevent use of any filtering or compensation during data processing. Hence, only direct signal recording can be used. At the beginning of our experiment, the absorption sensitivity achieved was $\alpha_{\min} = 3 \times 10^{-3}$ [16]. In this respect it is necessary to mention that the maximum ethanol absorption α for the highest ethanol partial pressure presented in Fig. 8 was equal to 0.077. Variations in recorded absorption were much smaller (see Fig. 6). During the experiment it was found that several processes were responsible for sensitivity limitation: intensity variations, environmental water interference and inhomogeneity of the laser beam (see below). All these processes had similar orders of magnitude.

Let us consider the minimum detectable absorption for experiments presented in the previous section. The minimum detectable ethanol partial pressure $P_{\min} = 0.16$ Torr obtained for the calibration test and bubbling technique corresponds to an absorption sensitivity (4), $\alpha_{\min} = 9.1 \times 10^{-6}$ for a measurement time of 0.5 s. This value characterizes the instrument and method in use. Results obtained are more than three orders of magnitude better in comparison with previous results. The improvement was achieved due to the above-mentioned analytical spectral range change, laser frequency tuning stabilization, and the orthogonalization procedure reducing interference with water absorption. Absorption sensitivity of the rapid monitoring mode was found to be $\alpha_{\min} = 2.5 \times 10^{-5}$. This experimental result is close to the 2.1×10^{-5} value calculated based on ADC resolution and data processing in use.

As a $10^{-5} - 10^{-6}$ sensitivity level is considered as our nearest goal, it is necessary to take into account the next physical limiting process. In [13] it was demonstrated that the basic limitation of trace absorption detection using a TDL is related to the physical properties of the TDL itself. The TDL active area has inhomogeneous properties: excitation current density (see Sect. 2.3), random radiation defect locations and temperature and strain distributions, etc. Laser electromagnetic standing waves interact with this inhomogeneous active area to produce laser radiation with a given intensity, frequency, polarization, near-field intensity and phase distribution on the laser facet.

For other excitation currents, the overlapping of the standing wave and inhomogeneous active area will be different. Hence, when the TDL excitation current is changed, one will observe small variations in all the laser radiation parameters mentioned above. Some of them (frequency and intensity variations) were observed experimentally [28]. For trace-molecule detection, variations in intensity (baseline) and laser beam are of the main importance. Increasing baseline variations when a diaphragm was installed in the laser beam described above was due to change in near-field laser radiation with excitation current. Some of these problems were solved by single-mode fiber usage, which made the TDL beam homogeneous (for example, all long-term instabilities mentioned in Sect. 3.1 were due to laser beam instability). However, the basic problem of the baseline remains valid because it is related to internal TDL properties. Typical variations in the baseline during laser pulses observed in our experiments were of the order of $10^{-3} - 10^{-4}$ and were reproducible on a short timescale. For the rapid monitoring mode, the baseline can be subtracted using the recorded reference signal. On a long timescale, the inhomogeneous laser structure is unstable because of temperature fields, strains, etc. changing. As a result, the baseline form is also changed. The characteristic time for such changes is of the order of a few minutes. This fact explains the above-mentioned flicker-type limitation for TDL sensitive absorption detection. Several approaches developed to solve the baseline problem (to be published elsewhere) promise to achieve $10^{-7} - 10^{-8}$ absorption detection sensitivity levels.

Characteristics of the DL radiation pattern are of great importance for the problem under consideration. To investigate TDL intensity distribution, a small diaphragm (1 mm in diameter) was installed in the collimated laser beam (with a diameter around 15 mm) after the objective (see Fig. 4). The diaphragm was mounted on a two-coordinate translation stage with micrometric feedings and could be installed at any point in the laser beam. The instrument operated in the same mode as that presented in Fig. 6a. Additional reproducible variations in the analytical signal ($\sim 1\%$) similar to baseline variations in [28] were observed with the diaphragm installed. It was supposed that the TDL beam inhomogeneity was responsible for this effect. To characterize this inhomogeneity, we measured the ratio of the signals from two data sets near the end of the pulse (ratio of signals corresponding to different excitation currents). This ratio has to be the same at any point in a homogeneous laser beam. The experimental ratio distribution is shown in Fig. 11. The chart only contains areas where the recorded signal was more than 5% of its maximum value. In the vertical direction perpendicular to the laser $p-n$ junction, the beam is rather homogeneous. In the horizontal direction ($x-$axis) in the plane of the junction it is very inhomogeneous, the above-mentioned ratio changed from 2.2 on left side to 1.6 on right. In other words, laser radiation for different currents had dif-

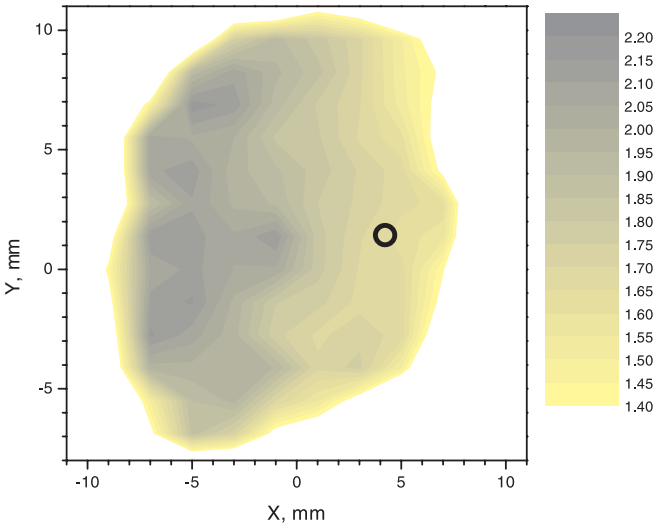

FIGURE 11 Laser radiation diagram inhomogeneity, *circle* shows diaphragm dimension (see text)

ferent near-field intensities and phase distributions on the laser facet (location, dimension, fine structure), and the same for the far-field region – direction of beam propagation, its dimension and wavefront form depend on laser excitation current.

For detection of trace broadband absorbers, these effects are very dangerous because any small change in the optical scheme (change in optical alignment, atmosphere turbulence, etc.) will cause large disturbances in the analytical signal. This assumption was checked experimentally. The photodiode was aligned to obtain maximum signal when all radiation was focused on its sensing area (no diaphragm was used) and a reference signal was recorded. Then the photodiode was gradually displaced in four directions to have half of the previous signal and the right, up, down and left parts of the laser beam were recorded by the photodetector. The analytical signal $A(i)$ obtained is presented in Fig. 12. As can be seen, the disturbances were as big as 1%. Similar to Fig. 11, disturbances in the vertical direction are smaller in comparison with the horizontal direction.

To overcome the effect of inhomogeneous TDL beam, several approaches can be proposed: 1 – to develop a TDL with a smaller dimension in the plane of its $p-n$ junction to prevent laser near-field radiation variations with excitation current; 2 – to install a small diaphragm in the beam to make the transmitted part of the beam more homogeneous; 3 – to use a scattering screen to make radiation recorded by the photodetector more homogeneous, etc. In the last two cases, significant reduction of recorded signal will take place. The most attractive approach to obtain homogeneous laser radiation is related to the employment of a TDL coupled with a single-mode fiber. Figure 13 demonstrates a test of this assumption. The measurement procedure was the same as for Fig. 10. Two TDL modules were used in this experiment. The first module, with a laser similar to the one used in previous experiments, was installed in the experimental set-up (left). A dramatic increase in noise ($\alpha_{\min} \sim 2 \times 10^{-3}$) was observed when the laser beam was crossed by a glass plate. We used glasses with different qualities. Different types of disturbances were observed: interference fringes dominated for high-quality glass with parallel surfaces, while for a low-quality glass, a deflection in the direction of beam propagation was observed when the glass crossed the laser beam. The results presented were obtained with the second type of glass plate. The results we

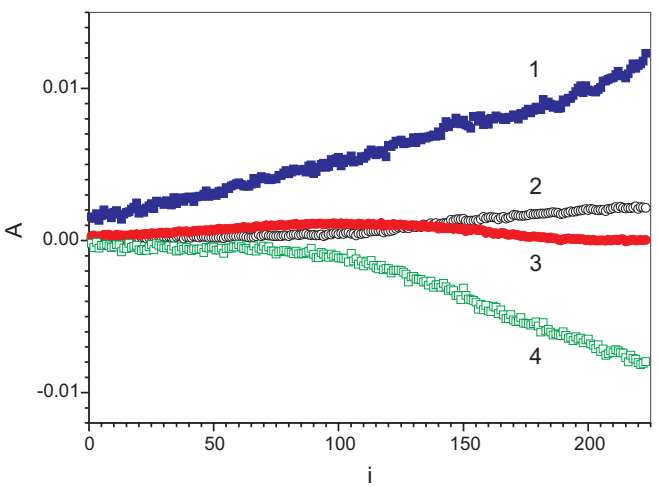

FIGURE 12 Analytical function $A(i)$ for photodiode displacements in different directions with respect to its initial position: 1, right; 2, up; 3, down; 4, left

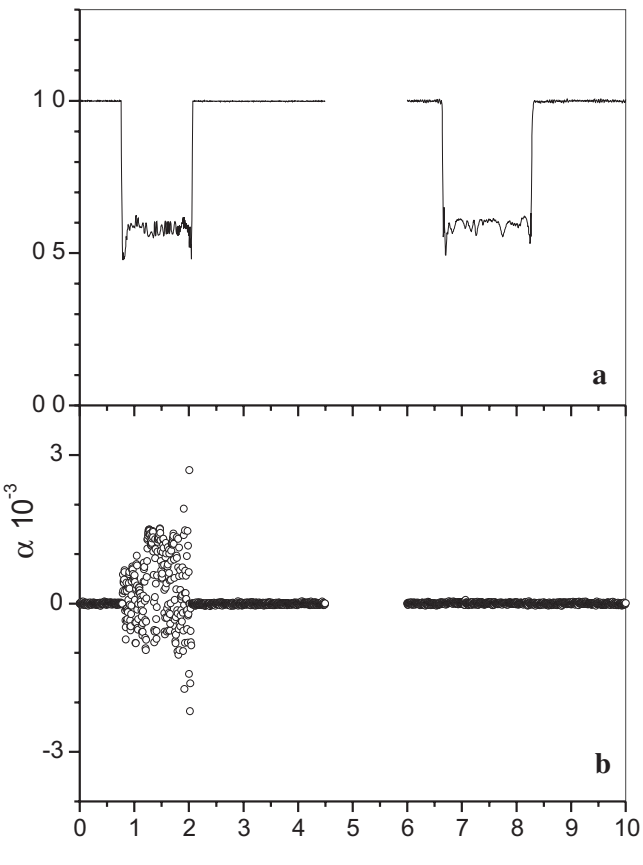

FIGURE 13 Transmission T (**a**) and absorption – α (**b**) measurements when laser beam was crossed by a glass plate: diode laser (*left*), diode laser coupled to single-mode fiber (*right*)

obtained obviously take into account the above considerations, because laser beam deflection has to produce a signal waveform variation if the beam is inhomogeneous. A homogeneous laser beam was obtained when the TDL in use was coupled to a single-mode fiber. TDL radiation was focused on the fiber facet by a spherical lens. Experimental results with this TDL module are presented in Fig. 13 (right). In spite of significant recorded intensity variations, the great absorption sensitivity improvement is obvious. Minimum absorption sensitivity $\alpha_{\min} \sim 4.8 \times 10^{-5}$ was measured. The value we obtained corresponds to a minimum detectable integrated concentration of $C_{\min} L = 88$ ppm $\times$ m (4). It is two times worse in comparison with results presented in Fig. 10 because more detailed investigation showed the presence of a disturbance correlated with the transmission signal.

8 Field tests

The technique presented above was developed for particular applications; several are presented below. Figure 14 shows the first demonstration of the possibility of measuring trace ethanol vapor concentration inside a moving car passing through the laser beam. The instrument and scattering screen were installed on opposite sides of the road. Data acquisition and processing were the same as for Fig. 13. In transmission T one can easily observe the car structure. From left to right: front window, driver window, driver head, driver seat, rear window, etc. This experiment took place before we were able to use a TDL coupled with a single-mode fiber. A scattering screen was used to make the laser beam more homogeneous (see above). However, it is obvious that the result obtained was worse in comparison with the single-mode fiber used to obtain a homogeneous laser beam. Because car windows deflected the laser beam, which remained partially inhomogeneous, the disturbances we observed were large. Significant signal reduction due to the scattering screen produced high noise for 100% transparency time intervals. We determined a minimum detectable integrated concentration $C_{\min} L = 350$ ppm $\times$ m sensitivity in this experiment, which is not enough, but reaching higher sensitivity in this case was not our goal. This was the first field test of an instrument and approach developed for rapid remote monitoring of trace complex molecules (broadband absorbers). Two events are presented in Fig. 14. In the first case (left), when the car passed the laser beam, no ethanol was detected inside. Before the second event was recorded, some ethyl alcohol was evaporated inside the car and an ethanol concentration of 630 ppm was measured.

The next example of a field test is presented in Fig. 15. We used an instrument [22], the detailed description of which is the subject of a forthcoming publication. The instrument was installed in the corridor of our building. TDL light was scattered from a wall located at 45 m from instrument. A mirror (15 cm in diameter) collected scattered light on an InGaAs photodiode. Data processing similar to Fig. 9 with a 500-μs signal period and 600 averages was used in this experiment. The figure presents *CL* – integrated propane concentration. At the beginning of the experiment no propane concentration was detected at a level of 1 ppm. The sensitivity for this type of instrument is determined by photodiode noise because the recorded scattered laser light is very small (around 1–5 nW). At a given time, 13 : 56 : 15, a propane-containing volume was opened and a few liters of propane were freed towards laser beam. When the beam was crossed by the gas flow, a narrow spike was generated. To understand the form of the *CL* behavior, it is necessary to remember that the experiment took place in a long corridor. After crossing the laser beam, propane flow

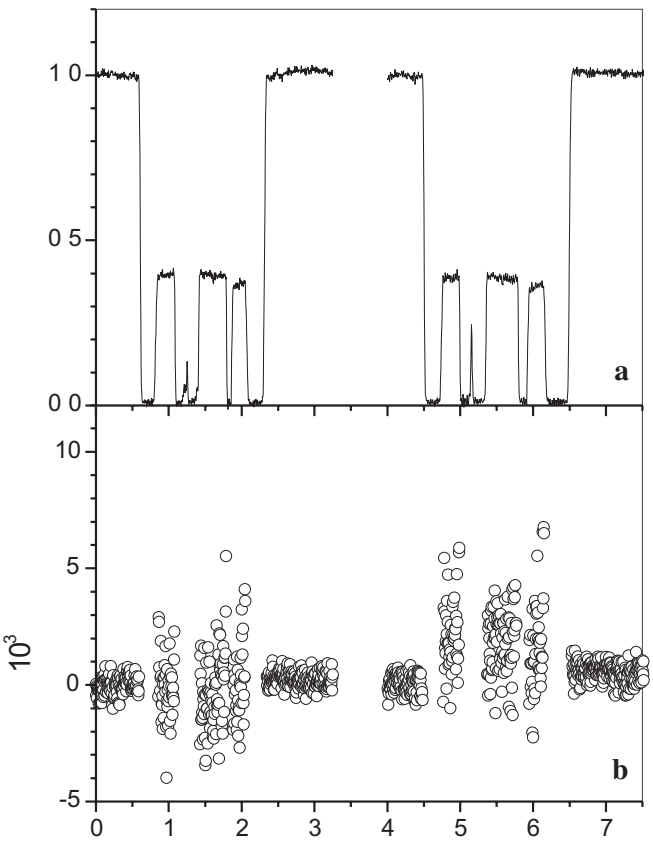

FIGURE 14 Transmission, T (**a**) and *CL*, ethanol integrated concentration (**b**) measurements when laser beam was crossed by moving car without (*left*) and with ethanol vapor inside (*right*)

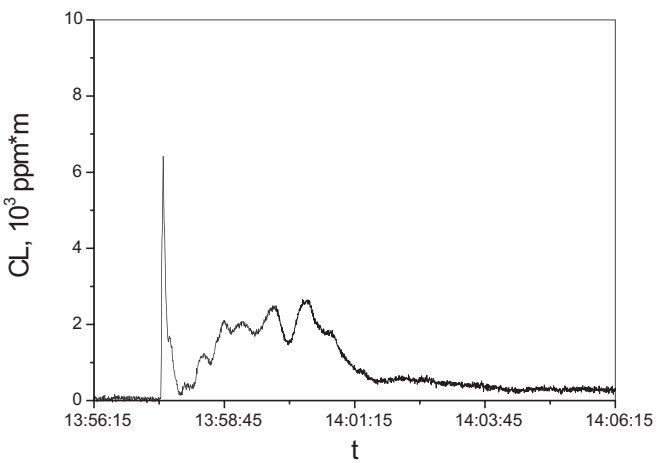

FIGURE 15 Propane leakage detection using instrument developed and topography reflector at 45 m distance

reached the corridor wall, was reflected, and after some time propane again appeared in the laser beam (broad maximum with *CL* variation). At some time the propane concentration was the same in the whole corridor cross-section. After this moment, the instrument detected constant integrated concentration with a value depending only on the propane leakage volume.

9 Conclusion

In the present paper we describe new hardware, software and data-processing approaches for trace complex-molecule detection. Different physical processes limiting sensitivity were considered and solutions were developed to reduce the mechanisms which influence instrument operation. Absorption sensitivity of the rapid-monitoring mode of the instrument developed was demonstrated to be $\alpha_{\min} = 2.5 \times 10^{-5}$ for trace complex-molecule detection and measurement time 4.5 ms. Taking $L = 500$ m if either a "Chernin" multipass cell [29] or an open path with retro reflector is used, the minimum detectable absorption coefficient $æ_{\min} = 4.8 \times 10^{-10}$ can be considered as being realistic for trace complex-molecule detection with a measurement time in the ms range, provided that a spectral range is chosen so that atmospheric absorption can be avoided. Achieved absorption sensitivity is good even in comparison with "small" molecule detection. The sensitivity limit was mainly determined by the 12-bit resolution of ADC in use. Averaging of signal trains can provide at least 10-times improvement in $\alpha_{\min}$ for a 0.5-s measurement time. The first results of the application of the developed technique for monitoring trace complex molecules in-field are presented.

ACKNOWLEDGEMENTS The present paper is dedicated to the memory of Prof. A. Prokhorov who initiated TDLS research in our Institute and supported it for decades. This work was partly supported by Brookhaven National Laboratory, Aquila Technologies Group, Inc. (Albuquerque, USA), and Pergam Company (Moscow, Russia). The authors wish to thank Dr.D.B. Stavrovskii and T.A. Shubenkina for FTS spectra recording; and Dr.M.V. Spiridonov and Y.P. Shapovalov for electronics development.

REFERENCES

1 E.D. Hinkley: Appl. Phys. Lett. **16**, 351 (1970)
2 Special issues of Spectrochimica Acta Part A, Guest eds. A.W. Mantz, A.I. Nadezhdinskii **52** (7), (1996) **55** (10), (1999) **58** (9), (2002) in press
3 R.T. Ku, E.D. Hinkley, J.O. Sample: Appl. Opt. **14**, 854 (1975)
4 J. Reid, J. Shewchun, B.S. Garside, A.E. Ballik: Appl. Opt. **17**, 300 (1978)
5 H.I. Schiff, G.I. Mackay, J. Bechara: In: *Air Monitoring by Spectroscopic Techniques*, ed. by M.W. Sigrist (Wiley, New York 1994)
6 D.M. Sonnenfroh, M.G. Allen: Appl. Opt. **35**, 4053 (1996)
7 P. Werle: Spectrochimica Acta Part A **54**, 197 (1998)
8 G. Durry, G. Megie: Appl. Opt. **38**, 7342 (1999)
9 A.A. Kosterev, A.L. Molinovsky, F.K. Tittel, C. Gmachl, F. Capasso, D.L. Sivco, J.N. Bailargeon, A.L. Hutchinson, A.Y. Cho: Appl. Opt. **40**, 5522 (2001)
10 I.I. Zasavitskii, Y.V. Kosichkin, A.I. Nadezhdinskii, E.V. Stepanov, A.Y. Tischenko, A.P. Shotov: Kratkie Soobscheniya po Physike **9**, 13 (1983) (in Russian)
11 I.I. Zasavitskii, Y.V. Kosichkin, A.I. Nadezhdinskii, E.V. Stepanov, A.Y. Tischenko, V.U. Khatatov, A.P. Shotov: Fresenius' J. Anal. Chem. **10**, 1903 (1985) (in Russian)
12 G.G. Devyatikh, I.I. Zasavitskii, Y.V. Kosichkin, G.A. Maximov, A.I. Nadezhdinskii, A.M. Prokhorov, E.V. Stepanov, A.Y. Tischenko, A.Y. Khomutov, A.P. Shotov, S.M. Schapin: Pis'ma JTF 11 **10**, 595 (1985) (in Russian)
13 I.I. Zasavitskii, A.I. Nadezhdinskii: In: *Monitoring of Gaseous Pollutants by Tunable Diode Lasers*, Vol. 95 ed. by R. Grisar, H. Preier, G. Shmidtke, G. Restelli (D. Reided Publishing Company, Dordrecht, Holland 1987) p. 176
14 A.I. Nadezhdinskii, E.V. Stepanov, I. I .Zasavitskii: Proc. SPIE **1724**, 238 (1992)
15 A.A. Kosterev, R.F. Curl, F.K. Tittel, C. Gmachi, F. Capasso, D.L. Sivco, J.N. Baillargeon, A.L. Hutchinson, A.Y. Cho: Appl. Opt. **39**, 4425 (2000)
16 A. Nadezhdinskii, A. Berezin, Y. Bugoslavsky, O. Ershov, V. Kutnyak: Spectrochim. Acta Part A **55**, 2049 (1999)
17 K.L. McNesby, R.T. Wainner, R.G. Daniel, A.W. Miziolek, W.M. Jackson, I.A. McLaren: Appl. Opt. **39**, 5006 (2000)
18 A. Mantz: private communication
19 G. Totschnig, D.S. Baer, J. Wang, F. Winter, H. Hofbauer, R.K. Hanson: Appl. Opt. **39**, 2009 (2000)
20 Code of Federal Regulations, Title 21, Vol. 8, Part 1040 – Performance Standards for Light-Emitting Products, Sec. 1040.10 Laser products; http://www.access.gpo.gov/nara/cfr/index.html
21 A.I. Nadezhdinskii, M.V. Spiridonov, Y.Y. Ponurovskii: private communication
22 Such an instrument was developed in our laboratory in collaboration with "Pergam Inc" firm (RF) and was tested during spring 2001, to be described elsewhere
23 A. Nadezhdinskii: Spectrochim. Acta Part A **52**, 959 (1996)
24 O.M. Bulashenko, J.M. Rubi, V.A. Kochelap: Appl. Phys. Lett. **73**, 217 (1998)
25 L. Rothman, C. Rinsland, A. Goldman, S. Massie, J.M. Flaud, A. Perrin, V. Dana, J.Y. Mandin, J. Schroeder, A. McCann, R. Gamache, R. Wattson, K. Yoshino, K. Chance, L. Brawn, V. Nemtchinov, P. Varanasi: *The HITRAN Molecular Spectroscopic Database and HAWKS (HITRAN Atmospheric Workstation)*, 1996 edn.
26 I. Zasavitskii, A. Kuznetsov, Y. Kosichkin, P. Krukov, A. Nadezhdinskii, A. Perov, E. Stepanov, A. Shotov: Pis'ma v JTF **8**, 1168 (1982) (in Russian)
27 R. Thompson: J. Chem. Edu. **74**, 532 (1997)
28 A. Nadezhdinskii, Y. Ponurovskii, M. Spiridonov: IEEE J. Quantum Electron. **QE-29**, 916 (1999)
29 S.M. Chernin: Infrared Phys. Technol. **37**, 87 (1996)